Clocked atom delivery to a photonic crystal waveguide

A. P. Burgers[a,1], L. S. Peng[a,1], J. A. Muniz[a,2], A. C. McClung[a,3], M. J. Martin[a,4], and H. J. Kimble[a,5]

[a]Norman Bridge Laboratory of Physics, California Institute of Technology, Pasadena, CA 91125

Contributed by H. J. Kimble, November 7, 2018 (sent for review October 8, 2018; reviewed by Julien Laurat and Vladan Vuletic)

Experiments and numerical simulations are described that develop quantitative understanding of atomic motion near the surfaces of nanoscopic photonic crystal waveguides (PCWs). Ultracold atoms are delivered from a moving optical lattice into the PCW. Synchronous with the moving lattice, transmission spectra for a guided-mode probe field are recorded as functions of lattice transport time and frequency detuning of the probe beam. By way of measurements such as these, we have been able to validate quantitatively our numerical simulations, which are based upon detailed understanding of atomic trajectories that pass around and through nanoscopic regions of the PCW under the influence of optical and surface forces. The resolution for mapping atomic motion is roughly 50 nm in space and 100 ns in time. By introducing auxiliary guided-mode (GM) fields that provide spatially varying AC Stark shifts, we have, to some degree, begun to control atomic trajectories, such as to enhance the flux into the central vacuum gap of the PCW at predetermined times and with known AC Stark shifts. Applications of these capabilities include enabling high fractional filling of optical trap sites within PCWs, calibration of optical fields within PCWs, and utilization of the time-dependent, optically dense atomic medium for novel nonlinear optical experiments.

nanophotonics | atoms | quantum optics | surface forces

The integration of ultracold atoms with nanophotonic devices leads to strong atom–photon interactions that not only quantitatively advance quantum optics but also create qualitatively new paradigms for atom–photon interactions (1–3). Owing to small optical loss and tight confinement of the electromagnetic field, nanoscale devices are capable of mediating long-range atom–atom interactions by way of optical photons in the guided modes (GMs) of the structures. In a complementary fashion, long-range interactions between photons can be mediated by underlying lattices of atoms in 1D and 2D dielectric structures (4–6). With advanced fabrication capabilities brought on by nanophotonics, such physical processes provide novel possibilities for quantum communication, computation, networks, and metrology, as well as for quantum phases of light and matter (1–6).

Compared with the rapidly expanding theoretical literature, to date experimental progress has been more modest in integrating atoms and nanophotonics. Important laboratory systems include optical nanofibers, where $\simeq 10^3$ atoms have been trapped $\simeq$220 nm from fiber surfaces (7–11). Dispersion-engineered photonic crystal cavities (12, 13) and waveguides (14, 15) have achieved strong atom–photon coupling, albeit with only a few atoms trapped $\simeq$150 nm from dielectric surfaces. A grand challenge for this emerging field remains the laboratory attainment of 1D and 2D atomic lattices with high filling fraction and strong coupling of single atoms and photons within the GMs of the nanophotonic structures.

For the photonic crystal waveguides (PCWs) considered here, strong atom–field coupling requires devices designed for atomic physics that provide both stable atom trapping and large atom–photon coupling at the atom-trapping sites (1, 16). In the optical domain, suitable PCWs have lattice constant $a \simeq 350$ nm for dielectric constant $\epsilon \simeq 4$. Single-atom localization with optical traps inside vacuum voids of unit cells then constrains far-off resonance traps [FORTs (17)] to volume $(\Delta x, \Delta y, \Delta z) = (30, 100, 140)$ nm for energy of 100 μK, where x is along the waveguide, y is along the 250-nm vacuum gap direction, and z is perpendicular to the waveguide. Free-space atoms must be transported to and cooled within these tiny FORTs. Such transport, cooling, and trapping of atoms near and within nanoscopic dielectric structures requires adaptations of existing techniques from atomic physics (18–21), as well as the invention of new protocols, such as hybrid vacuum–light traps (1, 16).

Thereby motivated, in this article we describe various investigations aimed at developing better quantitative understanding and new tools for the control of atomic motion under the influence of optical and surface forces near nanophotonic PCWs, as illustrated in Fig. 1. An important goal of this research is to formulate and validate in situ diagnostics that enable atoms to be conveyed from free space into GM optical traps within a PCW, ultimately with high fractional filling of each lattice site.

More specifically, our system shown in Fig. 1 consists of a quasi-1D PCW whose band structure arises from periodic modulation of the outer edges of two parallel dielectric beams with a central vacuum gap, resulting in the so-called "alligator photonic crystal waveguide" ("APCW") (14, 15, 22). A moving optical lattice transports trapped atoms into and through the APCW with velocity $v_{\text{lattice}} = 0.51$ m/s and temperature $T_{\text{lattice}} \simeq 20$ μK. Synchronous with the moving lattice, transmission spectra are recorded as functions of lattice transport time and detuning of weak GM probes. Due to the periodicity of the lattice delivery, the recorded spectra can be offset in time by integer multiples of the lattice period and coherently combined to create

Significance

Traditional atom–light coupling techniques have propelled the field of quantum optics and atomic physics. Now, by drawing on spectacular improvements in nanofabrication and nanophotonics, we advance a different platform for studying atom–light interactions. The data and simulations presented here are a first step in understanding how cold atoms are delivered to these nanophotonic structures.

Author contributions: A.P.B., L.S.P., J.A.M., M.J.M., and H.J.K. designed research; A.P.B., L.S.P., J.A.M., A.C.M., and M.J.M. performed research; A.P.B., L.S.P., and A.C.M. contributed new reagents/analytic tools; A.P.B. and L.S.P. analyzed data; and A.P.B., L.S.P., and H.J.K. wrote the paper.

Reviewers: J.L., Laboratoire Kastler Brossel, Sorbonne Université; and V.V., Massachusetts Institute of Technology.

The authors declare no conflict of interest.

[1]A.P.B. and L.S.P. contributed equally to this work.

[2]Present address: JILA, University of Colorado, Boulder, CO 80309.

[3]Present address: Department of Electrical and Computer Engineering, University of Massachusetts Amherst, Amherst, MA 01003.

[4]Present address: Physics Division, Los Alamos National Laboratory, Los Alamos, NM 87545.

[5]To whom correspondence should be addressed. Email: hjkimble@caltech.edu.

This article contains supporting information online at www.pnas.org/lookup/suppl/doi:10.1073/pnas.1817249115/-/DCSupplemental.

Published online December 26, 2018.

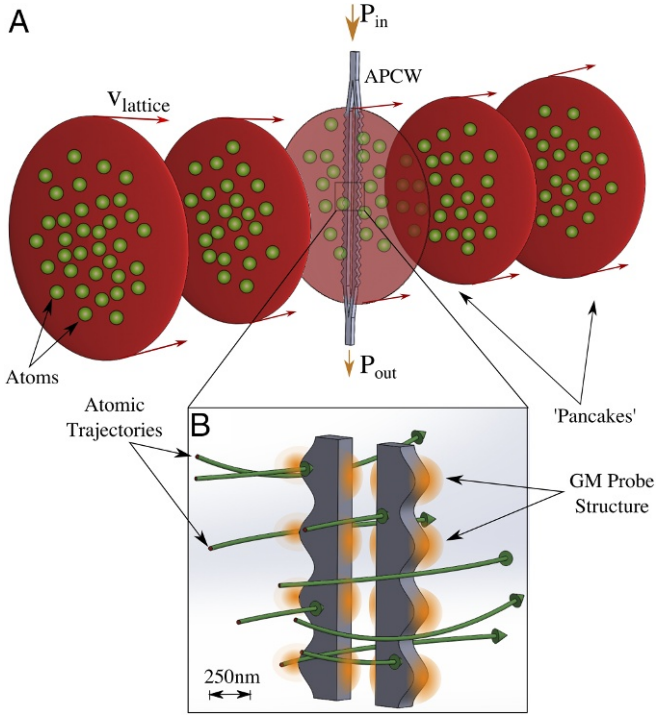

Fig. 1. (*A*) Atomic delivery to the APCW in our experiment is achieved by creating an optical conveyor belt from a 1D free-space lattice. The atoms, trapped in "pancakes" of high laser intensity, are transported to the device at a speed $v_{lattice}$ and interact transiently with the APCW. The atomic signature is read out through changes in the transmission of a weak, near-resonant probe ($P_{in} \rightarrow P_{out}$) that is an electromagnetic mode of the waveguide. (*B*) Depiction of atom trajectories showing the transient nature of the atoms as they pass through and around and "crash" into the APCW. The bright probe modes on the "teeth" and center of the APCW illustrate the transverse electric-like (TE-like) GM intensity near a TE band edge [here the dielectric band edge at ≃894 nm (D1 line of cesium)]. While these trajectories are merely an illustration, calculated atomic trajectories are presented along with comparisons to experimental data in Fig. 4.

time-dependent "clocked spectra" with temporal (spatial) resolution of ≃100 ns (≃50 nm).

These measurements allow us to quantitatively validate our numerical simulations and thereby provide understanding of atomic trajectories passing around and through nanoscopic regions of the APCW. For example, we infer that the number of atoms transported into the 250-nm-wide vacuum gap of the APCW during each lattice period is of order unity (i.e., $\sim 10^6$ atoms/s into the central vacuum gap). Introducing auxiliary GM fields provides a spatially varying AC Stark shift, which can control atomic trajectories arriving to the central vacuum gap at predetermined times and with known AC Stark shifts.

This quantitative understanding of atomic transport through the nanoscopic APCW provides more tools for the integration of ultracold atoms and nanophotonics, some of which we describe here. For example, following ref. 21, we consider the transfer of atoms from the moving optical lattice into GM trap sites along the APCW by way of single-photon scattering events triggered by the temporal phase of the moving lattice.

The research reported in this paper has many important antecedents in atomic physics. Historic measurements of transmission for atomic beams passing through nanofabricated arrays of slits led to some of the first observations of interferometry with atomic deBroglie waves that were followed over the next decades by precision measurements of many fundamental atomic properties (ref. 23 for a review), including atom–surface interactions important to our work. Pioneering experiments to measure atomic line shifts and decay rate modifications for atoms near surfaces were also made in other microscopic geometries with atomic transmission recorded through various structures (24–26), which are likewise quite relevant for our system. Early work in atomic vapors led to measurements of the spectral line distortion for Cs atoms induced by surface forces on the atoms (27–29). More recent experiments have investigated the role of Casimir–Polder (CP) forces on simulated trajectories of thermal (∼300 K) atoms interacting with nanoscopic slot waveguides and accompanying experiments verifying the importance of CP when explaining the experimental result (30). Among many experiments with laser-cooled atoms, landmark measurements of CP forces were made by "bouncing" atoms from evanescent fields (31), as well by using interactions with Bose–Einstein Condensates (BECs) at controlled distances from a dielectric boundary, again with atom loss being the relevant variable (32, 33). Perhaps closest in spirit and implementation to the present work are pioneering experiments and numerical simulations for cold atoms moving near nanoscopic optical fibers (34), microtoroid resonators (35, 36), and PCWs (37) in which light transmission and reflection from the respective optical structures were used to link experiment and numerical simulation of atomic motion, rather than by direct atomic detection.

PCW and Supporting Structure

This section provides an overview of the APCW used in our experiments, including the relevant GMs of the waveguide, the coupling of light into and out of these GMs, and the structural support of the waveguide. More details about device fabrication and characterization can be found in refs. 22, 38, and 39.

The APCWs used in our experiments are made by patterning the desired geometry using electron beam lithography on a 200-nm-thick layer of silicon nitride (SiN) grown on a 200-μm silicon substrate, followed by various stages of chemical processing (38, 39). The photonic crystal is formed by external sinusoidal modulation of two parallel nanobeams to create a photonic bandgap for TE modes with band edges at the strong dipole-allowed transition lines of cesium (Cs), the D1 line near 894 nm and the D2 line near 852 nm. Fig. 2*A* displays a scanning-electron microscope (SEM) image of the central section of an APCW. The "X" and "O" points indicate regions of high GM intensity for TE-polarized light with frequencies near the dielectric (D1) and air (D2) band edges, respectively. The coordinate system adopted for our subsequent analyses is shown together with the dimensions of the device and the principal polarizations of relevant GMs supported by the dielectric structure. Calculated and measured dispersion relations for such devices are presented in ref. 15 where good quantitative agreement is found.

Fig. 2*B* provides a cross-section of the two dielectric beams that form the PCW overlaid with intensity profiles for the transverse magnetic-like (TM-like) and transverse electric-like (TE-like) polarizations for the x coordinate corresponding to the widest sections of the APCW. Note that the TM mode's regions of highest intensity are on the top and bottom surfaces of the dielectric, while the TE mode is primarily bright in the center (vacuum gap between the beams) and on the sides. For operation near the band edges of the TE mode, spontaneous emission rates, Γ_{1D}, into the waveguide are strongest for atoms coupled to TE GMs ($\Gamma_{1D}/\Gamma' \leqslant 10$) and significantly weaker for emission into TM GMs (15, 22). Additionally, near the TE band edges for D1 and D2, the Bloch functions develop high-contrast standing waves along x, which are useful for creating dipole trapping potentials (FORTs) for atoms within the waveguide (16, 22). The TM GMs near D1 and D2 have low contrast in the x direction and resemble simple GMs of an unstructured waveguide. *SI Appendix*, Fig. S7 shows these modes and the resulting trapping potentials.

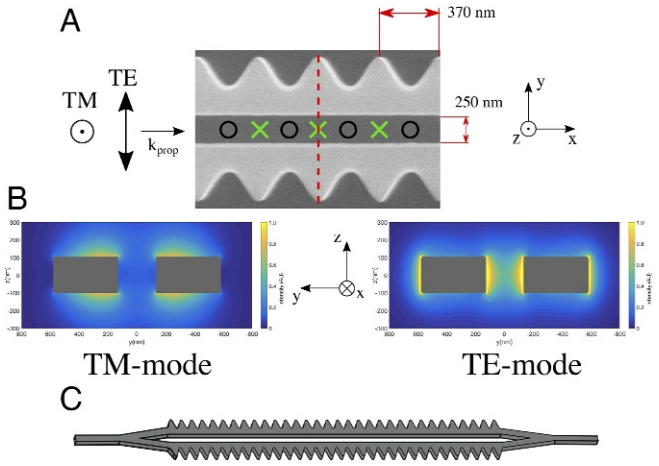

Fig. 2. Details of the APCW used in our experiments. (*A*) An SEM image of 4 unit cells of the APCW taken in the center region of the waveguide. The unit cell spacing is 370 nm, the vacuum gap between the beams is 250 nm, and the silicon nitride is 200 nm thick. Xs (Os) indicate the regions of the APCW where TE-guided light at the dielectric or D1 (air or D2) band egde is brightest. (*B*) The intensity distribution of the TE and TM polarizations supported by the structure at a single slice in the *y* direction, indicated by the red dashed line in *A*. (*C*) The 150 unit cells of the APCW are formed from single rectangular waveguides on either end that split at Y junctions into parallel, modulated beams. The entire structure is suspended in vacuum by transverse tethers connected to supporting side rails (not shown) (22, 38, 39).

The structure depicted in Fig. 2*C* illustrates the APCW connected to single-beam waveguides on either end and thereby suspended in the center of a 2-mm-wide window in the silicon chip to allow optical access for delivering and manipulating cold atoms near the APCW. Well beyond the ends of the APCW, a series of tethers are attached transversely to the single-beam waveguides along $\pm y$ to anchor the waveguides to two side rails that run parallel to the x axis of the device to provide thermal anchoring and mechanical support.

Light is coupled into and out of the GMs of the APCW by conventional optical fibers that are mode matched to the fields to/from the terminating ends of the waveguide (22). The overall throughput efficiency from input fiber through the device with the APCW to output fiber is $\sim$20% for the experiments described here.

The silicon chip containing a set of APCWs is affixed to a ceramic holder using heat-cured, low out-gassing glue. Each of eight devices is connected using separate input and output fibers aligned to the respective waveguide by V grooves etched into the substrate (22). The same heat-cured glue is used to fix the fiber position within the V groove. This entire assembly with 16 coupling fibers for eight devices is mounted in a vacuum chamber $\sim$20 mm from a magneto-optical trap (MOT) from which cold cesium atoms are transported to an individual APCW by way of an optical conveyor belt described in the next section.

Periodic Atom Delivery and Probe Measurements

Previous experiments with strong coupling of atoms to nanophotonic structures have relied upon tight focusing of FORTs (17) to confine a single atom (12, 13) or several atoms (14, 15) 100–200 nm above nanophotonic cavities and waveguides. To further investigate atomic motion and atom–field interactions near nanophotonic devices, our current approach uses a moving optical lattice that repetitively delivers atoms to the surfaces and central vacuum gap of a nanoscopic APCW. Although each lattice period results in of order one atom entering the central vacuum gap of the APCW, a recursive scheme for transferring atoms from the moving lattice to stationary FORT sites within the APCW could create a 1D lattice of single atoms with high fractional filling in time $\sim 10^{-3}$ s (e.g., a sequence of 1,800 lattice periods each lasting $\sim$1 μs), as is discussed in the next section. Each atom thereby trapped within a unit cell would couple to single GM photons within the waveguide with interaction rate $\Gamma_{1D} \sim$10 times larger than previous schemes with similar devices (14, 15, 22).

The moving optical lattice of trapped atoms is prepared by loading a 1D dipole trap from atoms confined in a MOT using polarization gradient cooling (PGC) (40). The dipole trap is formed using two counterpropagating TEM_{00} laser beams (B_1, B_2), each with waist $w_0 \simeq 60$ μm at the device and red detuning from the Cs D2 line by $\Delta_{\text{lattice}} \simeq 2\pi \times 800$ GHz. The atoms are thus trapped in a series of pancakes around intensity maxima along z with spacing at $\lambda_{\text{laser}}/2$. For each experimental trial, $\simeq 2 \times 10^6$ atoms are loaded into the free-space lattice and the spatial extent of the atomic sample spans $\sim$1,800 pancakes. After the atoms are loaded into the 1D lattice, polarized perpendicular to the waveguide (linearly polarized along y), we use degenerate Raman sideband cooling (DRSC) to cool the atomic sample to $T \simeq 12$ μK (41).

Beams (B_1, B_2) are derived from a single laser beam that is split into two paths each with a double-pass 80-MHz acousto-optic modulator (AOM). A frequency chirping sequence is sent to one of the AOMs to create a moving optical lattice (42), which acts as an optical conveyor belt to deliver atoms to the APCW at a speed given by the lattice spacing $\lambda_{\text{laser}}/2$ and the chirp frequency f_{chirp}, $v_{\text{lattice}} = f_{\text{chirp}} \times \lambda_{\text{laser}}/2$. For the experiments discussed here, the frequency difference between B_1 and B_2 is ramped from zero up to $f_{\text{chirp}} = 1.2$ MHz, corresponding to an atom delivery speed of $v_{\text{lattice}} = 0.51$ m/s. The relevant diagram for loading and delivering atoms to the APCW with this conveyor-belt technique is found in *SI Appendix*.

The atomic interaction with the APCW is probed using a weak resonant field of frequency ω_{probe} input to either a TE or a TM GM of the waveguide. In qualitative terms, atoms located within 100–200 nm from the surfaces of the APCW result in additional absorption and/or dispersion for a probe field transmitted at ω_{probe} relative to the device with no atoms. By recording transmission spectra obtained by scanning ω_{probe} around a particular free-space Cs transition at frequency ω_a, we obtain quantitative information related to light shifts of transition frequencies and modified decay rates that atoms experience in transiting near the structure (15). More precise understanding of atomic trajectories on scales $\lesssim$50 nm and $\lesssim$100 ns can be gained by using the periodic arrival of atoms by the moving optical lattice supplemented by auxiliary, far-from-resonance GM fields that strongly perturb internal atomic states and thus atomic motion.

"Clocked" Transmission Spectra

By using the lattice delivery method illustrated in Fig. 3 *A, i* and *A, ii*, atoms arrive to the APCW trapped in a sequence of pancakes, with the repetition frequency of arrivals given by f_{chirp} and periodicity $\tau_{\text{lattice}} = 1/f_{\text{chirp}}$. During the passage of any one pancake, a small fraction ($\sim 10^{-8}$) of the lattice power is scattered by device imperfections into GMs of the APCW and propagates to both ends, where it is efficiently coupled into optical fibers and then separated from the probe fields using volume Bragg gratings (VBGs) (8). The leaked lattice light (with a power of $\sim$5 nW) is detected by an avalanche photodiode (APD), with the resulting current observed with high signal-to-noise ratio and contrast (i.e., oscillating from near zero to a sequence of maxima with contrast $\simeq$0.7 and period τ_{lattice} to provide a "fringe signal"). The photocurrent is directly digitized and recorded with a field programmable gate array (FPGA), as well as processed in real

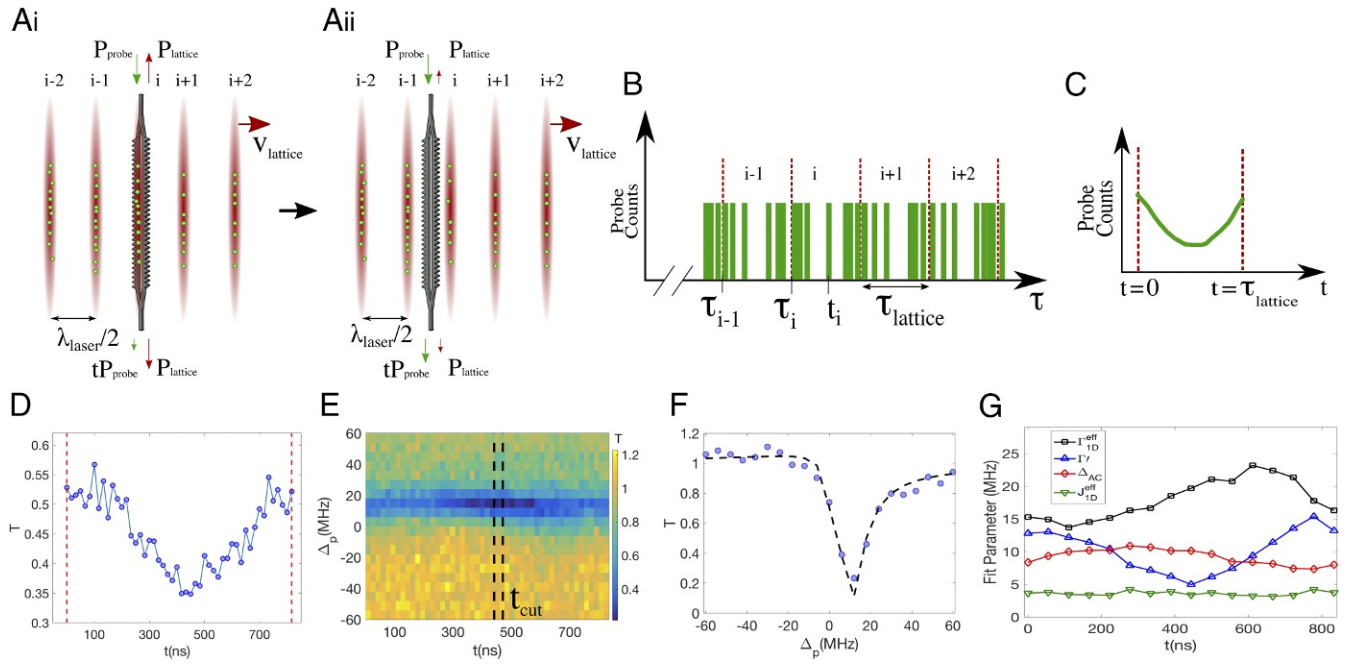

Fig. 3. Details of the concept of the clocked-atom delivery and how the data are analyzed to recover a phase-sensitive atomic signal. (*A, i*) Atoms trapped in pancakes by the 1D lattice are delivered to the structure when a chirp sequence is placed on one of the lattice beams creating a conveyor belt. (*A, ii*) A half period later the pancakes have moved $\lambda_{laser}/4$ relative to the APCW. (*B*) Probe photon counts placed on the same time axis as the lattice sync signal. By building a histogram from probe time stamps (t_i) between successive lattice sync time stamps (τ_i, τ_{i-1} . . .) we can recover the phase-sensitive nature of the atom delivery. (*C*) All of the individual lattice time periods are folded together into a single histogram indicating that the atomic signature is phased with the lattice signature. (*D*) For a single probe detuning we can observe this clear phase-sensitive signal when the probe photon time stamps are referenced to the closest preceding time stamps of the lattice. (*E*) By scanning the probe detuning we can create this 2D image in lattice time t and probe detuning Δ_p to gain more insight into the arrival time of different classes of atoms and extract spectra for various arrival times. This information helps to determine the coupling of the atoms to the waveguide and can reveal time-dependent AC Stark shifts. Cuts at certain times reveal spectra which we fit to extract parameters $\{\Gamma_{1D}^{eff}(t), \Gamma'(t), \Delta_{AC}(t), J_{1D}^{eff}(t)\}$ for an effective model. (*F*) An example of slices taken over an interval "t_{cut}" and summed. (*G*) The fit parameters extracted for spectra at varying lattice times t in *E*. Each spectrum is taken by combining three time bins ($\simeq$50 ns) and fitting to a transmission model given in ref. 15 and *SI Appendix*. Note that Γ_{1D}^{eff} changes the most across time and denotes the coupling strength of the atomic sample to the structure. J_{1D}^{eff}, the coherent coupling term, remains relatively constant and small across time.

time using a threshold detector that converts the fringe signal to a single time marker for each pancake, which we call the lattice synchronous markers, defined as τ_i (i.e., the red dashed lines in Fig. 3*B* at time $i \times \tau_{lattice}$ for the ith pancake). These synchronous markers provide a consistent clock to register time stamps of each (separately) detected probe photon transmitted by the APCW (i.e., green bins in Fig. 3*B*) with the movement of the lattice through the structure. The random nature of the device imperfections on both the top and bottom can alter the timing of the lattice scattering into the APCW relative to the atom arrival. While this introduces a level of uncertainty, it manifests as a global phase offset which is consistent for all measurements on a single device, but can vary between different waveguides as discussed in *SI Appendix*.

The transmitted probe counts, recorded on a single-photon counting module (SPCM) and digitized, from the passage of each lattice pancake can then be offset in time by lattice number (i.e., for pancake i, $t_{i,clock} = t_i - \tau_i$, where $\tau_i = i \times \tau_{lattice}$) and summed over all pancakes $\{i\}$ to produce a clocked record as illustrated schematically in Fig. 3*C*, where t refers to the clocked time for a sequence of N_p pancakes passing near the APCW. Histograms built from the time differences between the lattice time stamps and the probe time stamps reveal microscopic information about atom motion near the APCW. For example, Fig. 3*D* displays a measured histogram that clearly evidences the phase-sensitive nature of the atom arrival for a single-probe detuning matching the free-space Cs D1 transition $F = 3 \rightarrow F' = 4$. In Fig. 3 and throughout this paper, the probe transmission with atoms is normalized to the transmission through the waveguide when no atoms are present. The use of the Cs D1 transition for probing instead of the D2 cycling transition is to avoid the tensor shifts of the D2 excited states that arise from the lattice detuning from the D2 line. For lattice period $\tau_{lattice} = 833$ ns, minimum transmission (i.e., maximum loss) is observed around the clocked time $t \simeq 450$ ns, corresponding to increased atom number near the APCW as in Fig. 3 *A, i*. By contrast, maximum transmission (and minimum loss) is evident near $t = 0, 833$ ns as in Fig. 3 *A, ii* with lattice antinodes (and hence atom number for a red detuned FORT) located away from the device.

To gain greater insight into atomic motion and internal state shifts for atoms near the APCW (e.g., AC Stark shifts and resulting forces), we create 2D clocked spectra by combining measurements as in Fig. 3*D* for a sequence of probe detunings, $\Delta_p = \omega_{probe} - \omega_a$. For each value of Δ_p, time bins of recorded probe counts over the lattice period with atoms present are normalized to the probe counts at the same detuning but absent atoms in the lattice. Fig. 3*E* provides an example of measured 2D clocked spectra for a weak TM probe beam. For each detuning Δ_p of the probe beam, typically 5–10 trials of the experiment are combined, with each trial consisting of 1,800 lattice pancakes and repeated every 2 s.

Cuts of the 2D spectra along lines of varying probe detuning Δ_p for fixed clock times t (i.e., times relative to the lattice synchronization signal) can exhibit distinct spectra resulting from spatially dependent atomic density and coupling strength of atoms to the APCW. An example of a transmission spectrum at $t_{cut} = 450$ ns is shown in Fig. 3*F*. Following the discussion in

SI Appendix, we fitted the measured clocked transmission spectra to an effective model that was developed in refs. 15 and 43 for a random number of atoms trapped above a 1D PCW and moving along x. The three fitted parameters for this effective model are Γ_{1D}^{eff} and J_{1D}^{eff}, which describe effective decay rates and frequency shifts, respectively, for N-atom radiative interactions with the measured GM (TE or TM), as well as Γ' for single-atom decay into all other modes (principally free-space modes), which is assumed to have no collective effects (44).

The coupling strengths $\{\Gamma_{1D}^{\text{eff}}(t), J_{1D}^{\text{eff}}(t)\}$ and decay rate $\Gamma'(t)$ are extracted as functions of the clocked lattice time t (*SI Appendix*). Fig. 3*G* provides an example of such temporal behavior of $\{\Gamma_{1D}^{\text{eff}}(t), J_{1D}^{\text{eff}}(t), \Gamma'(t)\}$ over a lattice period. Here $\Gamma_{1D}^{\text{eff}}(t)$ changes over time, reflecting the atom density and coupling to the structure in a lattice period. $J_{1D}^{\text{eff}}(t)$ remains relatively constant, indicating a small contribution from atom–atom interactions, which is unsurprising given that these experiments are taken far from the dielectric band edge where the coherent coupling term is small. This technique thereby provides otherwise inaccessible information about radiative interactions along the APCW as pancakes of atoms move through the device.

Clocked Spectra with Stark GMs

For the previously described clocked spectra, atoms experience spatial and temporal variations of AC Stark shifts $\Delta_{AC}^{\text{lattice}}(r,t)$ due to the complex structure of the optical fields of the moving optical lattice and CP forces in the vicinity of the APCW, which are considered in more detail in *Simulations of Atom Motion and Clocked Spectra*. In this section we investigate experimentally clocked transmission spectra in the presence of a far-detuned GM that produces its own spatial distribution of AC Stark shifts $\Delta_{AC}^{\text{GM}}(r,t)$ near the surfaces of the APCW, as illustrated by the TM and TE GM mode profiles shown in Fig. 2*B*. The GMs here are launched incoherently from each fiber port of the APCW to avoid the large vector shifts on the atomic energy levels. We achieve this incoherent sum by detuning one of the GMs by 100 MHz which is a fast enough beat note that the atomic motion is unaffected, but not fast enough compared with the overall GM detuning of 58 GHz to create any appreciable difference from the point of view of the atoms (i.e., an atom interacting with a GM detuned by 58 GHz behaves similarly to one interacting with a 58.1-GHz detuned GM).

As shown in Fig. 4 *A–D*, the addition of static GM fields leads to 2D clocked spectra with much richer structure than absent these fields. The measured spectra exhibit variations in transmission on timescales $\delta t \simeq 100$ ns and associated length scales $\delta z \simeq 50$ nm for lattice velocity of 0.51 m/s, under the influence of a TM GM with power range $0 \leqslant P_{Stark} \leqslant 92$ μW and blue detuning of 58 GHz from the D2 line (referred to from now on as the "TM Stark GM"). The configuration of the involved beams is presented in *SI Appendix*, Fig. S4. The corresponding peak AC Stark shifts in the vacuum spaces surrounding the APCW are estimated to be $0 \leqslant \Delta_{AC}^{\text{GM}} \leqslant 50$ MHz, bounded by the kinetic energy of the atoms imposed by the lattice speed. Here, the atoms enter in $F=3$ and the probe beam is tuned around the $F=3 \rightarrow F'=4$ transition of the D1 line of Cs (with free-space frequency ω_a), again to avoid inhomogeneous broadening associated with the D2 excited-state tensor shifts from the free-space optical lattice.

In the presence of the TM Stark GM for the measurements in Fig. 4 *A–D*, atoms experience a repulsive dipole force and the atomic transition frequency is shifted smaller than that of free space. Atoms arriving to the side of the APCW facing the incoming moving lattice begin to climb up the repulsive potential created by the blue TM Stark GM and lose kinetic energy.

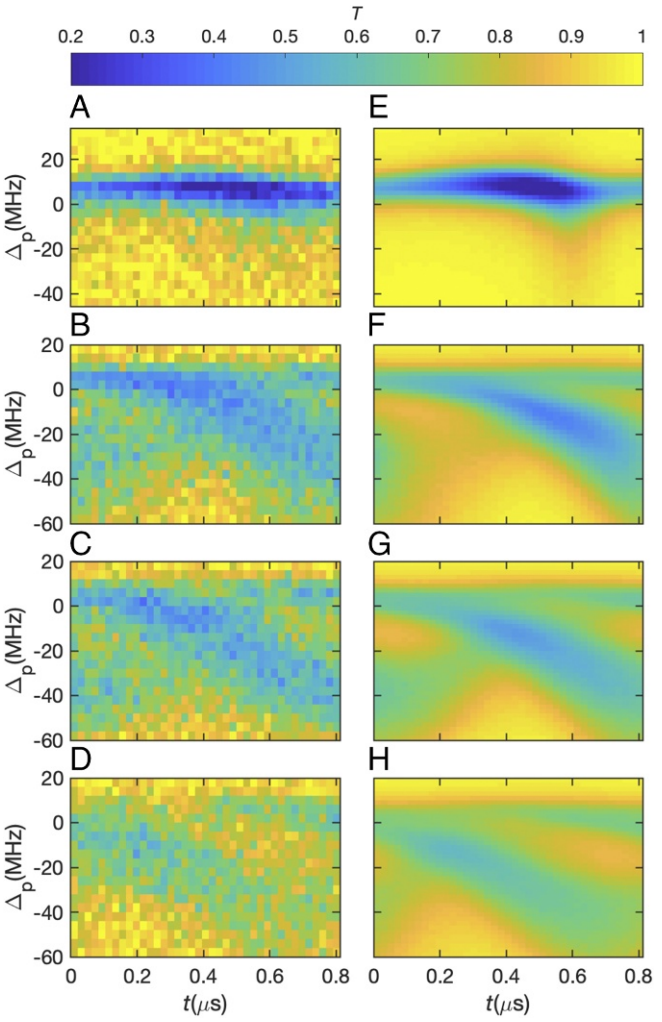

Fig. 4. (*A–H*) A comparison of the data (*A–D*) and simulation (*E–H*). In both cases, there are two TM GMs of the APCW being excited, namely (*i*) a weak TM probe beam with variable frequency ω_p and detuning $\Delta_p = \omega_p - \omega_a$, with ω_a the free-space frequency of the $F=3 \rightarrow F'=4$ transition in the D1 line of atomic Cs, and (*ii*) a counterpropagating pair of TM stark GMs with a sequence of increasing powers from zero (*Top*). The configuration of the involved beams is presented in *SI Appendix*, Fig. S4. For the measurements in *A–D*, the sequence of input powers is $P_{Stark} = \{0, 42, 66, 92\}$ μW from *Top* to *Bottom*, while for the simulations in *E–H*, from *Top* to *Bottom*, the internal power sequence is $P_{Stark} = \{0, 12.6, 19.8, 27.6\}$ μW for the GM detuning of 58 GHz from $F=3$ on the D2 line. As the simulated TM Stark beam power is increased the atomic sample response alters in both time and detuning in ways similar to increasing the power in the simulation. This allows the intensity of GMs to be calibrated by comparing the data and simulation.

As atoms climb this potential, the AC Stark shift they experience increases due to the spatial intensity of the TM Stark GM. Evident in the data is that atom arrivals at different times exhibit different Stark shifts.

Moving to higher power for the TM Stark GM in Fig. 4 *A–D*, we observe an evolution of atomic signatures where atoms arriving at different times within one pancake experience different Stark shifts. A temporally varying atomic signature on the scale of ≃100 ns, while itself of interest, can be used to determine the arrival time of atoms and their spatial distribution around the surfaces of the APCW. This information cannot be extracted from the data alone, but when aided by numerical simulations and validations, can enable "actionable" information to be obtained from the measured clocked spectra. In the next section we describe numerical simulations of

atom delivery and clocked spectra, with the good correspondence between experiment and simulation already displayed in Fig. 4 *A–H*.

In principle we can choose any GM polarizations for the probe and Stark fields, as well as detuning and Stark shift, depending on the effect desired on the atomic signal. Clocked spectra for additional GM configurations (e.g., TE probe and TM Stark beam) can be found in *SI Appendix*. Additionally, here we focus on lattice speeds of 0.51 m/s; however, we can easily adjust this speed by changing the beat frequency between B_1 and B_2 and have experimentally investigated lattice speeds from 0.7 m/s down to 0.02 m/s.

Simulations of Atom Motion and Clocked Spectra

In this section, we present numerical simulations of atom trajectories and APCW transmission spectra. Numerical simulations of atom motion in a moving optical lattice and through the near fields of the APCW can be used to understand the nanoscopic dynamics of atoms near the APCW. Together with a model based upon optical transfer matrices for atoms located near the APCW, theoretical simulations for clocked transmission spectra can be generated for comparison with experiment, as in Fig. 4 *E–H*. Such simulations can also aid the design and operational validation of GM optical traps and test numerically techniques for loading small-volume ($(\Delta x, \Delta y, \Delta z) = (30, 100, 140)$ nm) GM traps in short times (~ 1 μs).

The simulations for atomic transport presented here are carried out in the 2D space of y, z to reduce the required computational resources and enable more rapid explorations of parameter space. Justification for this reduction from full 3D is that the lattice fields along x for full 3D simulations exhibit only small modulation ($\lesssim 5\%$), as is also the case for so-called side-illumination traps used in refs. 14 and 15.

For the current 2D simulations, the domain area extends ± 25 μm along y and from -10 μm to 60 μm along z in a plane that contains the thick part of the APCW (i.e., the red dashed line in Fig. 2*A*), with the center of the gap at the origin. The total time-dependent potential $U(t)$ for a single atom consists of three contributions: (*i*) $U_{\text{lattice}}(t)$ for the optical lattice that differs significantly from the usual case of free space due to forward and backward scattering from the APCW for each otherwise independent, counterpropagating lattice beam, with $U_{\text{lattice}}(t)$ simulated with the finite-element method (FEM) implemented in COMSOL (45); (*ii*) $U_{\text{GM}}(t)$ from GM fields externally input to the APCW, with $U_{\text{GM}}(t)$ determined from eigenmode calculations for the APCW GMs done with MPB (46); and (*iii*) U_{CP} from CP force originating from the interaction between the atoms and the dielectric surfaces (26). Atoms are initialized in U_{lattice} with a Boltzmann distribution for temperatures ranging over $10\ \mu\text{K} < T_{\text{initial}} < 150\ \mu\text{K}$ and for lattice depths $200\ \mu\text{K} < U_{\text{lattice}}^{\text{initial}} < 500\ \mu\text{K}$ at distance 60 μm from the APCW in z, where the scattered fields from the APCW are small. Atom trajectories are calculated by solving the classical equations of motion for the assumed independent atoms in the optical dipole potential $U(r,t) = U_{\text{lattice}}(r,t) + U_{\text{GM}}(r) + U_{\text{CP}}(r)$, which consists of the optical lattice, APCW GMs, and CP force. The CP force is important to include in these simulations; see Fig. 7 for a comparison graph consisting of Fig. 4 *A* and *E* and the simulation case where $U_{\text{CP}}(r)$ is removed. The result clearly indicates that, to achieve good agreement between simulation and data, CP force must be included in the overall potential felt by the atoms.

The simulated atomic trajectories near the APCW for a single pancake with initial loading temperature $T_{\text{initial}} = 100\ \mu\text{K}$ and no GM ($U_{\text{GM}} = 0$) are shown in Fig. 5*A*. Notable features include phase advances and retardations as each pancake nears and departs from the central plane of the APCW, which lead to atomic acceleration and deceleration, and a significant flux of atoms enter the central 250-nm vacuum gap of the APCW.

To calculate the APCW transmission spectrum as a function of time, the atom trajectories are randomly sampled according to the experimentally measured density of $\simeq 500$ atoms per pancake. The sampled atom trajectories are then distributed along the x direction with probability proportional to the probe intensity in the APCW. For example, for a TE probe with frequency near the APCW TE band edge, the atom trajectories are distributed with a $\cos^2(2\pi x/a)$ probability distribution, where a is the APCW unit cell spacing (370 nm), to approximate the high-contrast Bloch mode. For a TM probe with frequency near the Cs D1 or D2 transitions, the TM band edges are both far from the probe frequency (15) with low-contrast Bloch modes (i.e., effectively traveling waves), so that the atom trajectories are distributed uniformly along x. Since our GM probe field is far below saturation, the transmission of the system as a function of probe frequency can be calculated with the transfer matrix model (15, 43, 47).

For an initial loading of five consecutive pancakes, Fig. 5*B* shows the transmission spectrum of a weak TM probe $T(\Delta_p, t)$ calculated from the resulting simulated trajectories by way of a matrix transfer model. By applying the same analysis as previously described for our experiments (namely, folding the five pancake spectra into one optical lattice period), a clocked spectrum can be generated over the timescale τ_{lattice}, with the result shown in Fig. 5*C*. The clocked spectrum is also present in Fig. 4*E*.

The simulation results with a calculated blue detuned TM Stark GM are shown in Fig. 5 *D–F*. Note that the TM Stark GM alters the atom trajectories and induces the AC Stark shift in the transmission spectra. The blue detuned TM Stark GM allows atoms at different regions around the APCW to be separated by different AC Stark shifts, as evidenced in Figs. 4 and 5*F*, and two classes of atom trajectories can be identified: (*i*) atoms that go around the sides of the APCW, that experience little AC Stark shift from the TM Stark GM and remain trapped in the optical lattice standing wave; these atoms contribute to the horizontal strip around 8 MHz in Fig. 5*F*, as indicated by the blue dashed line; and (*ii*) atoms that interact with the APCW GM strongly on the surface facing the incoming atoms and in the vacuum gap of the APCW; these atoms contribute to the negative AC Stark-shifted feature in Fig. 5*F*. As atoms climb up the strong repulsive potential, the negative AC Stark shift increases, creating the downward sloping feature, indicated by the red dashed line in Fig. 5*F*. For atoms that bounce back or pass through the gap, the AC Stark shift decreases in magnitude, as indicated by the white dashed line in Fig. 5*F*. More insight into atom motion around the APCW can be extracted from the clocked spectrum as explained below.

A side-by-side comparison of the simulation and data is shown in Fig. 4. This not only demonstrates reasonable correspondence between simulation and data, indicating reliability of conclusions drawn from simulations, but also provides the ability to determine the actual intensity within the APCW, a vitally important piece of information when determining the optimum power for GM trap beams.

A more detailed description of the simulations can be found in *SI Appendix* along with links to movies of the atom delivery to the waveguide (Movies S1 and S2). Fig. 5 *A* and *D* shows snapshots at different times from Movies S1 and S2. Additionally, we explored the possibility of using a blue detuned lattice where the atoms are repelled from the regions of high intensity. For this blue lattice, the simulation indicates that the delivery of atoms to the center vacuum gap of the APCW is increased compared with that in the traditional red detuned lattice.

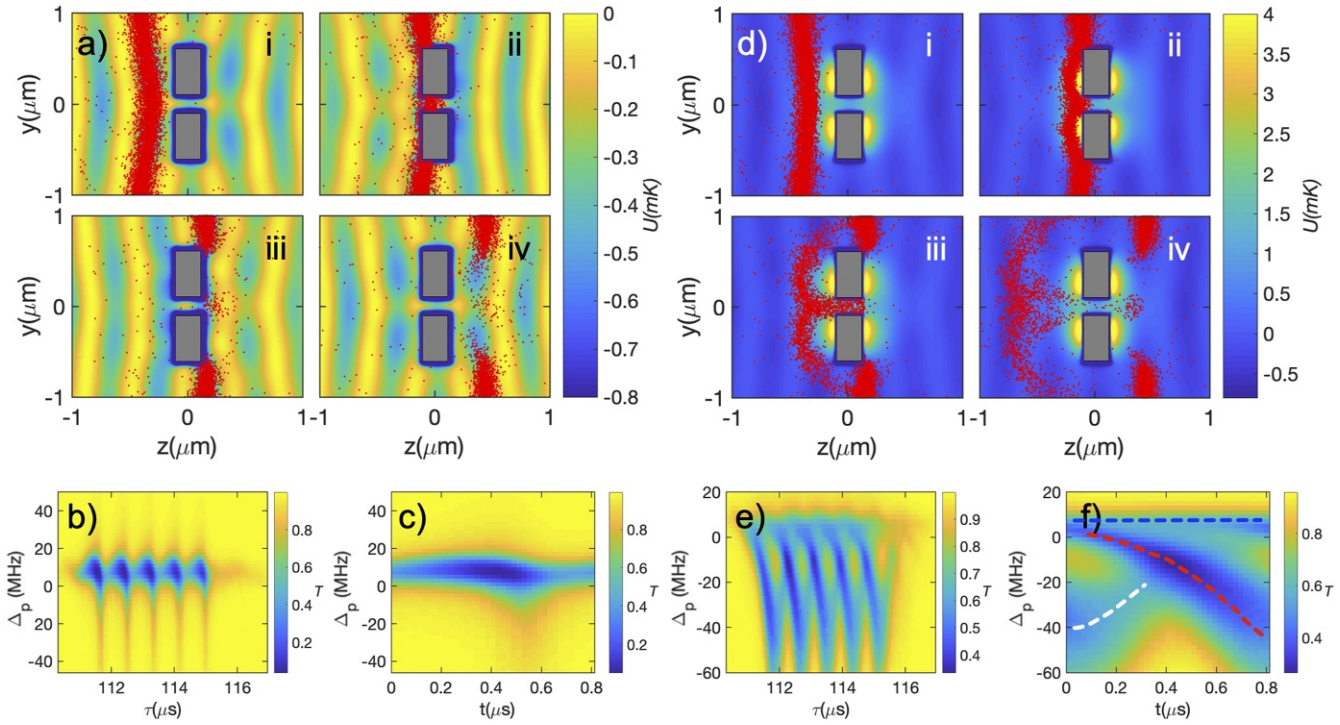

Fig. 5. Simulated atom delivery and the corresponding simulated clocked spectra. Note that the atom number in *A* and *D* is much larger per pancake than in the experiment to illustrate the multitude of trajectories a single atom could potentially follow. (*A*) The atomic trajectories without any APCW GM at four different times. The two gray rectangles are a cross-section at the thick part of the APCW, as indicated by the red dashed line in Fig. 2*A*. *A*, *i* shows atomic trajectories at $\tau = \tau_i$; *A*, *ii* those at $\tau = \tau_i + \frac{2}{3}\tau_{\text{lattice}}$; *A*, *iii* those at $\tau = \tau_{i+1} + \frac{1}{3}\tau_{\text{lattice}}$ (where $\tau_{i+1} = \tau_i + \tau_{\text{lattice}}$); and *A*, *iv* those at $\tau = \tau_{i+2}$. (*B*) By simulating multiple pancakes and sampling from the trajectories, a spectrum of multiple pancakes can be calculated. (*C*) A clocked spectrum generated by folding the multiple-pancake spectrum. Here the lattice configuration for clocked time $t = 0$ is shown in *A*, *i* and *A*, *iv* (i.e., the timing when the highest intensity of the lattice is at $z = 0$). (*D*) The atomic trajectories with an intense blue TM Stark beam. Timing is the same as in *A*. (*E*) The transmission spectrum for five pancakes with a blue TM GM. (*F*) Clocked spectrum with a blue TM Stark beam. Notable features of *D*, *E*, and *F* include the following: First, atoms that go around the sides of the APCW experience little AC Stark shift from the GM and remain trapped in the optical lattice standing wave; these atoms contribute to the horizontal strip around 8 MHz, indicated by the blue dashed line in *F*; and, second, atoms that interact with the APCW GM strongly on the surface facing incoming atoms and in the vacuum gap of the APCW; these atoms contribute to the negative AC Stark-shifted feature. As atoms climb up the strong repulsive potential, the negative AC Stark shift increases, creating the downward sloping feature, indicated by the red dashed line in *F*. And as the atoms bounce back or pass through the gap, the AC Stark shift decreases in magnitude, as indicated by the white dashed line.

Applications

Fig. 4 establishes strong correspondence between our measurements and simulations for various features of clocked spectra involving TM probe and TM Stark beams. Beyond the results in Fig. 4, we have made similar comparisons of clocked spectra for other pairs of GMs [e.g., (TE probe, TM Stark), (TM probe, TE Stark)], as described in Fig. 6 and *SI Appendix*. These results provide further validation of our numerical simulations, which are based upon calculated atomic trajectories as atoms brought by the moving lattice pass around and through nanoscopic regions of the APCW in the presence of forces from the lattice itself, Stark GMs, and surface forces. With a reasonable degree of confidence, we can then attempt to use the measured clocked spectra to provide insight into atomic trajectories that are currently beyond direct observation.

An example of the general intuition is as follows. As illustrated in Fig. 2*B*, a TM mode is primarily sensitive to atomic trajectories that intersect the top of the waveguide, while for the TE mode, the regions of highest intensity are on the sides and in the gap between the two beams. Hence, a TE probe can improve our sensitivity to gap and side atoms. To distinguish between these two classes of trajectories (side and gap), a TM Stark GM with blue detuning (as in Fig. 6 *A* and *B*) can be used to separate atoms interacting with the TE probe into two distinguishable classes. Because of the AC Stark shift and the spatial intensity distribution of the TM blue GM, an atom entering the vacuum the gap of the APCW will experience a larger AC Stark shift than an atom passing around the side. By validating this effect in our simulations, we can then use it to separate experimentally the side and gap classes of atoms in a clocked spectrum.

One important application is to use the lattice delivery method to achieve high fractional filling of the trap sites within the APCW by way of a recursive loading scheme (i.e., some small probability to transfer one atom from the moving lattice to a GM trap for the passage of each successive lattice pancake). Such recursive loading requires detailed understanding of the experimental signatures of atoms entering the central vacuum gap of the APCW, including the probability with which atoms actually enter the central gap. With the reliability of the simulations validated, we have some confidence in the result in Fig. 6 *A* and *B*, which shows that a significant fraction of atoms delivered to the APCW do indeed enter the vacuum gap under appropriate conditions of lattice speed and intensity for a TM Stark GM.

This being the case, the next step is to identify the operational signatures for the class of "gap" atoms in a clocked spectrum, which we have done in Fig. 6*C* by way of a TE probe GM. Here, the total clocked spectrum based upon all atom trajectories from the simulation is decomposed into a set of clocked spectra for individual trajectory classes, including the class of

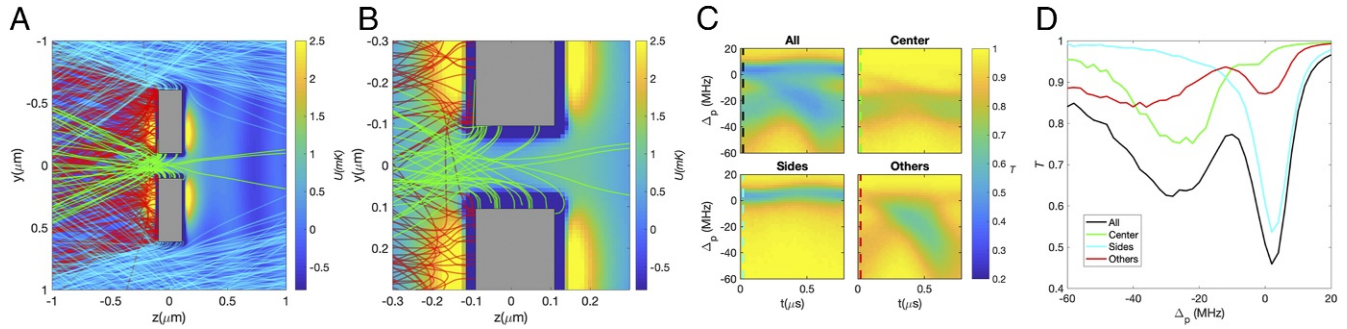

Fig. 6. (*A*) Different classes of atom trajectories with a TM blue detuned Stark beam. The green trajectories are the "center" trajectories that enter the gap of the APCW. The blue trajectories are the "sides" trajectories that go around the sides of the APCW. And the red trajectories are "other" trajectories that bounce from or crash on the surface facing incoming atoms of the APCW. (*B*) A zoomed-in view of the center gap showing atom trajectories entering the APCW. A large fraction of atoms penetrate deep into the gap before crashing into the dielectric wall via CP forces. (*C*) The clocked spectra for a TE probe of the different classes of atom trajectories shown in *A* and *B*. Note the separation of different classes in both time and AC Stark shift. (*D*) A cut at 20 ns in the clocked spectrum, as shown by the dashed lines in *C*. The black line shows the spectrum of all trajectories. The colored lines show the spectra of corresponding classes of trajectories in *A* and *B*. The spectrum for all atoms (black curve) has a large peak around probe detuning $\Delta_p \simeq -30$ MHz, which predominantly results from atoms entering the central gap. For these times and detunings, another GM could be triggered in real time to selectively target gap atoms (e.g., for trapping) while they transit the vacuum gap of the APCW in successive lattice pancakes.

trajectories that pass through the central vacuum gap. Fig. 6*D* zooms into the clocked spectrum by examining spectral cuts at successive time intervals to identify times and detunings for which the gap atoms have distinct spectral signatures. Clearly, the spectrum for all atoms (black curve) has a large peak around probe detuning $\Delta_p \simeq -30$ MHz, which predominantly results from atoms entering the central gap at clocked times around $t \simeq 20$ ns. For these times and detunings, another GM could be triggered in real time to selectively target gap atoms while they transit the vacuum gap of the APCW in successive lattice pancakes.

Inspired by ref. 21 for "single-photon cooling," we are attempting to adapt the capabilities illustrated in Fig. 6 for the transfer of atoms from the moving lattice into a GM trap by way of a single cycle of optical pumping (i.e., a single-photon scattering event) (48, 49). As depicted in *SI Appendix*, consider a moving lattice with FORT potential U_{lattice} and a TE-GM trap $U_{\text{GM}}(F)$ within the APCW having the property that $U_{\text{GM}}(F_1) \gg U_{\text{lattice}}$ for the ground manifold level F_1 and $U_{\text{GM}}(F_2) \lesssim U_{\text{lattice}}$ for level F_2, which for definiteness could be the $6S_{1/2}, F_1 = 3, F_2 = 4$ levels in cesium. Assume that atoms are being transported by a lattice with velocity v_{lattice} such that their kinetic energy is much less than $U_{\text{GM}}(F_1)$ and are prepared in F_2. Then by using techniques similar to those illustrated in Fig. 6, it should be possible to identify clocked time t and detuning Δ_{OP} at which to trigger a pulse of TE guided-mode light for optically pumping atoms $F_1 \to F_2$ within the central vacuum gap. Since the transfer involves momentum $\leqslant 2\hbar k$ and $U_{\text{GM}}(F_1) \gg U_{\text{lattice}}$, atoms should be trapped within $U_{\text{GM}}(F_1)$ as the lattice minimum exits the trap region. Furthermore, the choice of detuning, Δ_{OP}, for the optical pumping pulse allows discrimination in favor of atoms near the coincident minima of $U_{\text{GM}}(F_2)$ and $U_{\text{GM}}(F_1)$ [i.e., near the center of a (random) unit cell of the APCW] by way of AC Stark shifts as in Fig. 6.

Beyond this discussion of single-photon trapping, more practical applications of clocked spectra are already in place in our laboratory. Examples include the use of clocked spectra for intensity calibration within a GM of the APCW resulting from a known input power at the optical fiber coupled to the sequence of waveguides that lead to the actual APCW (22) and validation of trap parameters for GM traps formed from the summation of red and blue GMs (8, 16).

Certainly, the agreement between simulation and measurement can be considerably improved by extending the simulations to more faithfully capture the complexity of the APCW, including fully 3D lattice transport and vector fields of the APCW, and implementing more accurate calculations of CP potentials for all surfaces of the APCW as in ref. 16, which is nontrivial. Such improvements could enable more advanced measurements to be undertaken, such as quantitative validations of CP potentials in the spirit of refs. 23 and 50.

A full calculation of the CP potential of an atom around the nontrivial geometry of our dielectric structure is extremely involved and requires huge numerical resources. To simplify the calculation, the C_3 coefficients of short-range van der Waals atom–surface attraction for both Cs ground state and $6P_{1/2}$ excited state are taken from ref. 51. The CP potential for a single nanobeam in the APCW is approximated by considering only the atom–surface attraction force of the atom and its closest dielectric surface. However, as seen in Fig. 7, our current measurements are already sensitive to the C_3 coefficient chosen for the Cs $D1$ transition in our simplified van der Waals model (23, 52). This simple theory, although not complete, is nonetheless important in generating good correspondence between experiment and simulation. Finally, we note that achieving trapped atoms inside the structure will make our system more sensitive to surface forces. This will enable the ability to investigate CP potentials further and investigate deviations

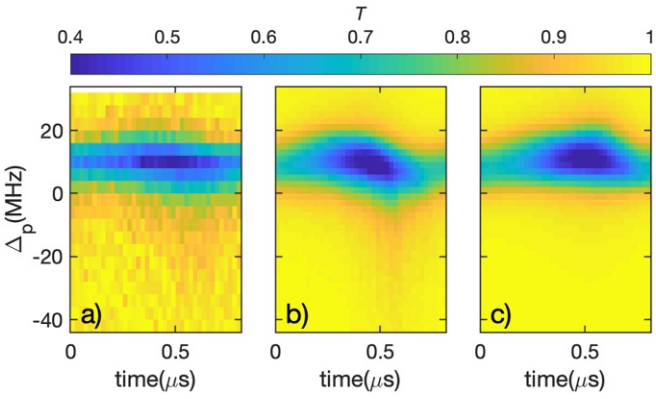

Fig. 7. (*A–C*) A comparison of clocked spectra for (*A*) experimental data, (*B*) simulation with the CP potential, and (*C*) simulation without the CP potential, for the case of no Stark GM and probing with a weak TM probe. The addition of the CP potential is essential for obtaining good correspondence between experiment and simulation.

due to additional surface forces such as the deposition of Cs atoms on the waveguide surface (We elaborate on this point in *SI Appendix*) (53).

A quite different application of our system of clocked atoms delivered to a PCW is utilization of this time-dependent, optically dense atomic medium for nonlinear optical experiments, such as soliton propagation, as investigated in ref. 54. The relevant pulse durations are much smaller than the atomic lifetime $\tau \simeq 30$ ns, which is in turn much shorter than the atom transit time through the APCW, so the pulses could be triggered to interact with an optical system with selected values of $\Gamma_{1D}^{\text{eff}}, J_{1D}^{\text{eff}}, \Delta_{AC}, \Gamma'$ as in Fig. 3*G* by varying the offset of input pulse and lattice clock timing.

In this nonexhaustive discussion of applications, we finally mention the possibility of opto-mechanics. In our modeling and experiments, the GM probe is kept weak to avoid affecting atomic motion as well as saturation, allowing modeling of optical transmission and reflection by way of matrix transfer techniques. That is, atoms strongly affect the probe response, but the probe only weakly affects atomic motion. On the other hand, the Stark GMs in the work presented are far detuned so that their transmission is only weakly modified by the atoms, but clearly atomic motion is strongly influenced by sufficiently intense Stark GMs, as in Fig. 5. Consider now that the probe and Stark GMs are one and the same field with intensity sufficient to drive atomic saturation as well as to create optical forces that modify atomic motion. We would then be in a regime requiring a self-consistent description of the internal and external degrees of freedom for atoms and optical fields within the APCW (i.e., a nonlinear regime for opto-mechanics with atoms). Although we have carried out such measurements with our current experiment, the results are beyond our existing simulation capabilities.

Conclusion and Outlook

Trapping and cooling atoms at distance $\sim$100 nm from the internal surfaces of dielectric PCWs requires a different set of advances relative to standard atomic physics techniques. Toward this end, we have described experiments and numerical simulations to understand better the motion of cold atoms under the influence of forces from GM fields within a PCW, external illumination with light transverse to the PCW axis, and CP interactions at the surfaces of the PCW. In particular, a moving optical lattice has been used to transport cold atoms to the surfaces and vacuum spaces of a nanoscopic PCW. By way of synchronous detection of the passing optical lattice and EM transmission spectra, we find rich phenomenology related to temporal and spatial variations of AC Stark shifts, radiative absorption from and emission into GMs, and (vacuum) surface forces, all of which strongly affect atomic motion.

In addition to empirical characterization of the resulting phenomena, we have carried out extensive numerical simulations in an attempt to achieve effective modeling tools with quantitative prediction capabilities, as well as provide physical insight. Initial validation of the simulations has been made by way of direct comparisons of simulated and measured clocked transmission spectra and reasonable correspondence has been achieved. By way of our simulations, we can then infer underlying characteristics of atomic motion and internal fields and, to some modest degree, control atomic dynamics within and near the PCW (e.g., maximizing the number of atoms that pass through the central vacuum gap of the PCW and providing operational signatures manifest in the associated clocked spectra).

Understanding the interplay of forces from GM traps, moving optical lattices, and surfaces of the APCW on the motion of atoms constitutes a significant step toward GM trapping of arrays of atoms within unit cells along the PCW. Under current experimental conditions, we estimate $\simeq$2 atoms per pancake delivered to the vacuum gap of the APCW. Since each experiment cycle delivers $\sim$1,800 pancakes, a modest trap transfer efficiency of 2% leads to $\sim$70 successful trapping events per cycle. Observations of single and collective radiative phenomena would then become possible in this engineered photonic environment, as described theoretically in refs. 1, 4, 5, and 55.

Throughout this paper, we have treated the atoms as classical point particles without interactions. Surely, at densities of 10^{12} atoms/cm^3, encountered around and within the APCW, these assumptions are no longer completely valid and a richer set of atomic interactions is accessible. Future experiments should investigate more carefully density-dependent effects, including inelastic hyperfine changing collisions and light-assisted collisions, which are critical for loading free-space optical tweezers (56, 57).

Moreover, we have ignored the wave character of the atoms (e.g., at $v_{\text{lattice}} = 0.51$ m/s the deBroglie wavelength $\lambda_{\text{dB}} \simeq 6$ nm). However, as the atomic velocity is reduced during cooling and trapping, λ_{dB} can become comparable to the dimensions of the vacuum spaces in the APCW (e.g., at 10 μK, $v_{\text{atom}} = 0.03$ m/s, and $\lambda_{\text{dB}} \simeq 100$ nm). In this regime, novel physics might be manifest as we arc back to the beginning of atom interactions with periodic nanostructures (23, 58).

Aside from trapping atoms in these nanostructures one can imagine specifically designed experiments tailored toward more precise measurements of CP forces at dielectrics surfaces. The ubiquity of the lattice delivery method does not require a structure as complicated as the APCW and in fact a more simple structure would ease the transition of our 2D simulations to a full 3D simulation model.

ACKNOWLEDGMENTS. We acknowledge sustained and important interactions with A. Asenjo-Garcia, J. B. Béguin, D. E. Chang and his group, A. Goban, J. D. Hood, C.-L. Hung, J. Lee, X. Luan, Z. Qin, and S.-P. Yu. We carried out the nanofabrication in the Caltech Kavli Nanoscience Institute and clean room of O. J. Painter, whom we gratefully acknowledge. H.J.K. acknowledges funding from the Office of Naval Research (ONR) Grant N00014-16-1-2399, the ONR Multidisciplinary University Research Initiative (MURI) Quantum Opto-Mechanics with Atoms and Nanostructured Diamond Grant N00014-15-1-2761, the Air Force Office of Scientific Research MURI Photonic Quantum Matter Grant FA9550-16-1-0323, the National Science Foundation (NSF) Grant PHY-1205729, and the NSF Institute for Quantum Information and Matter Grant PHY-1125565.

1. Chang D, Douglas J, González-Tudela A, Hung CL, Kimble H (2018) Colloquium: Quantum matter built from nanoscopic lattices of atoms and photons. *Rev Mod Phys* 90:031002.
2. Lodahl P, et al. (2017) Chiral quantum optics. *Nature* 541:473–480.
3. Pichler H, Choi S, Zoller P, Lukin MD (2017) Universal photonic quantum computation via time-delayed feedback. *Proc Natl Acad Sci USA* 114:11362–11367.
4. González-Tudela A, Hung CL, Chang DE, Cirac JI, Kimble H (2015) Subwavelength vacuum lattices and atom–atom interactions in two-dimensional photonic crystals. *Nat Photon* 9:320–325.
5. Hung CL, González-Tudela A, Cirac JI, Kimble HJ (2016) Quantum spin dynamics with pairwise-tunable, long-range interactions. *Proc Natl Acad Sci USA* 113:E4946–E4955.
6. González-Tudela A, Cirac JI (2017) Quantum emitters in two-dimensional structured reservoirs in the nonperturbative regime. *Phys Rev Lett* 119:143602.
7. Vetsch E, et al. (2010) Optical interface created by laser-cooled atoms trapped in the evanescent field surrounding an optical nanofiber. *Phys Rev Lett* 104:203603.
8. Goban A, et al. (2012) Demonstration of a state-insensitive, compensated nanofiber trap. *Phys Rev Lett* 109:033603.
9. Béguin JB, et al. (2014) Generation and detection of a sub-Poissonian atom number distribution in a one-dimensional optical lattice. *Phys Rev Lett* 113:263603.
10. Gouraud B, Maxein D, Nicolas A, Morin O, Laurat J (2015) Demonstration of a memory for tightly guided light in an optical nanofiber. *Phys Rev Lett* 114:180503.
11. Solano P, et al. (2017) Optical nanofibers: A new platform for quantum optics. *Advances In Atomic, Molecular, and Optical Physics*, eds Arimondo E, Lin CC, Yelin SF (Elsevier, London), Vol 66, pp 439–505.
12. Thompson JD, et al. (2013) Coupling a single trapped atom to a nanoscale optical cavity. *Science* 340:1202–1205.
13. Tiecke T, et al. (2014) Nanophotonic quantum phase switch with a single atom. *Nature* 508:241–244.
14. Goban A, et al. (2015) Superradiance for atoms trapped along a photonic crystal waveguide. *Phys Rev Lett* 115:063601.

15. Hood JD, et al. (2016) Atom–atom interactions around the band edge of a photonic crystal waveguide. *Proc Natl Acad Sci USA* 113:10507–10512.
16. Hung C, Meenehan S, Chang D, Painter O, Kimble H (2013) Trapped atoms in one-dimensional photonic crystals. *New J Phys* 15:083026.
17. Grimm R, Weidemüller M, Ovchinnikov YB (2000) Optical dipole traps for neutral atoms. *Advances in Atomic, Molecular, and Optical Physics*, eds Bederson B, Walther H (Elsevier, London), Vol 42, pp 95–170.
18. Dalibard J, Cohen-Tannoudji C (1989) Laser cooling below the Doppler limit by polarization gradients: Simple theoretical models. *JOSA B* 6:2023–2045.
19. Wieman CE, Pritchard DE, Wineland DJ (1999) Atom cooling, trapping, and quantum manipulation. *Rev Mod Phys* 71:S253–S262.
20. Phillips WD (1998) Nobel lecture: Laser cooling and trapping of neutral atoms. *Rev Mod Phys* 70:721–741.
21. Bannerman ST, Price GN, Viering K, Raizen MG (2009) Single-photon cooling at the limit of trap dynamics: Maxwell's demon near maximum efficiency. *New J Phys* 11:063044.
22. Yu SP, et al. (2014) Nanowire photonic crystal waveguides for single-atom trapping and strong light-matter interactions. *Appl Phys Lett* 104:111103.
23. Cronin AD, Schmiedmayer J, Pritchard DE (2009) Optics and interferometry with atoms and molecules. *Rev Mod Phys* 81:1051–1129.
24. Haroche S, Kleppner D (1989) Cavity quantum electrodynamics. *Phys Today* 42:24–30.
25. Sukenik C, Boshier M, Cho D, Sandoghdar V, Hinds E (1993) Measurement of the Casimir-Polder force. *Phys Rev Lett* 70:560–563.
26. Intravaia F, Henkel C, Antezza M (2011) *Fluctuation-Induced Forces Between Atoms and Surfaces: The Casimir–Polder Interaction in Casimir Physics* (Springer, Berlin), pp 345–391.
27. Oria M, Chevrollier M, Bloch D, Fichet M, Ducloy M (1991) Spectral observation of surface-induced van der Waals attraction on atomic vapour. *Europhys Lett* 14:527–532.
28. Chevrollier M, Bloch D, Rahmat G, Ducloy M (1991) Van der Waals-induced spectral distortions in selective-reflection spectroscopy of Cs vapor: The strong atom–surface interaction regime. *Opt Lett* 16:1879–1881.
29. Bloch D, Ducloy M (2005) Atom-wall interaction. *Advances in Atomic, Molecular, and Optical Physics*, eds Bederson B, Walther H (Elsevier, London), Vol 50, pp 91–154.
30. Ritter R, et al. (2018) Coupling thermal atomic vapor to slot waveguides. *Phys Rev X* 8:021032.
31. Landragin A, et al. (1996) Measurement of the van der Waals force in an atomic mirror. *Phys Rev Lett* 77:1464–1467.
32. Lin Yj, Teper I, Chin C, Vuletić V (2004) Impact of the Casimir-Polder potential and Johnson noise on Bose-Einstein condensate stability near surfaces. *Phys Rev Lett* 92:050404.
33. Obrecht JM, et al. (2007) Measurement of the temperature dependence of the Casimir-Polder force. *Phys Rev Lett* 98:063201.
34. Sagué G, Vetsch E, Alt W, Meschede D, Rauschenbeutel A (2007) Cold-atom physics using ultrathin optical fibers: Light-induced dipole forces and surface interactions. *Phys Rev Lett* 99:163602.
35. Stern N, Alton D, Kimble H (2011) Simulations of atomic trajectories near a dielectric surface. *New J Phys* 13:085004.
36. Alton D, et al. (2011) Strong interactions of single atoms and photons near a dielectric boundary. *Nat Phys* 7:159–165.
37. Goban A, et al. (2014) Atom–light interactions in photonic crystals. *Nat Commun* 5:3808.
38. Yu SP (2017) Nano-photonic platform for atom–light interactions. PhD thesis (California Institute of Technology, Pasadena, CA).
39. McClung AC (2017) Photonic crystal waveguides for integration into an atomic physics experiment. PhD thesis (California Institute of Technology, Pasadena, CA).
40. Kuppens S, Corwin K, Miller K, Chupp T, Wieman C (2000) Loading an optical dipole trap. *Phys Rev A* 62:013406.
41. Vuletić V, Chin C, Kerman AJ, Chu S (1998) Degenerate Raman sideband cooling of trapped cesium atoms at very high atomic densities. *Phys Rev Lett* 81:5768–5771.
42. Schrader D, et al. (2001) An optical conveyor belt for single neutral atoms. *Appl Phys B* 73:819–824.
43. Asenjo-Garcia A, Hood JD, Chang DE, Kimble HJ (2017) Atom-light interactions in quasi-one-dimensional nanostructures: A Green's-function perspective. *Phys Rev A* 95:033818.
44. Asenjo-Garcia A, Moreno-Cardoner M, Albrecht A, Kimble HJ, Chang DE (2017) Exponential improvement in photon storage fidelities using subradiance and "selective radiance" in atomic arrays. *Phys Rev X* 7:031024.
45. COMSOL (2017) *COMSOL Multiphysics Reference Manual*, version 5.3. Available at www.comsol.com. Accessed December 1, 2018.
46. Johnson SG, Joannopoulos JD (2001) Block-iterative frequency-domain methods for Maxwell's equations in a planewave basis. *Opt Express* 8:173–190.
47. Chang DE, Jiang L, Gorshkov A, Kimble H (2012) Cavity QED with atomic mirrors. *New J Phys* 14:063003.
48. Taïeb R, Dum R, Cirac J, Marte P, Zoller P (1994) Cooling and localization of atoms in laser-induced potential wells. *Phys Rev A* 49:4876–4887.
49. Falkenau M, Volchkov VV, Rührig J, Griesmaier A, Pfau T (2011) Continuous loading of a conservative potential trap from an atomic beam. *Phys Rev Lett* 106:163002.
50. Bender H, et al. (2014) Probing atom-surface interactions by diffraction of Bose-Einstein condensates. *Phys Rev X* 4:011029.
51. Failache H, Saltiel S, Fichet M, Bloch D, Ducloy M (2003) Resonant coupling in the van der Waals interaction between an excited alkali atom and a dielectric surface: An experimental study via stepwise selective reflection spectroscopy. *Eur Phys J D At Mol Opt Plasma Phys* 23:237–255.
52. Gregoire MD, Brooks N, Trubko R, Cronin AD (2016) Analysis of polarizability measurements made with atom interferometry. *Atoms* 4:21.
53. McGuirk JM, Harber DM, Obrecht JM, Cornell EA (2004) Alkali-metal adsorbate polarization on conducting and insulating surfaces probed with Bose-Einstein condensates. *Phys Rev A* 69:062905.
54. Kozhekin A, Kurizki G (1995) Self-induced transparency in Bragg reflectors: Gap solitons near absorption resonances. *Phys Rev Lett* 74:5020–5023.
55. Douglas JS, et al. (2015) Quantum many-body models with cold atoms coupled to photonic crystals. *Nat Photon* 9:326–331.
56. Schlosser N, Reymond G, Protsenko I, Grangier P (2001) Sub-Poissonian loading of single atoms in a microscopic dipole trap. *Nature* 411:1024–1027.
57. Kaufman AM, Lester BJ, Regal CA (2012) Cooling a single atom in an optical tweezer to its quantum ground state. *Phys Rev X* 2:041014.
58. Keith D, Schattenburg M, Smith HI, Pritchard D (1988) Diffraction of atoms by a transmission grating. *Phys Rev Lett* 61:1580–1583.